TM4SF5 Knockout Protects Mice From Diet-Induced Obesity Partly by Regulating Autophagy in Adipose Tissue

Cheoljun Choi,[1] Yeonho Son,[1] Jinyoung Kim,[1] Yoon Keun Cho,[1] Abhirup Saha[1], Minsu Kim,[1] Hyeonyeong Im,[1] Kyungmin Kim,[1] Juhyeong Han,[1] Jung Weon Lee,[1] Je Kyung Seong,[2] and Yun-Hee Lee[1]

Diabetes 2021;70:2000–2013 | https://doi.org/10.2337/db21-0145

Transmembrane 4 L six family member 5 (TM4SF5) functions as a sensor for lysosomal arginine levels and activates the mammalian target of rapamycin complex 1 (mTORC1). While the mTORC1 signaling pathway plays a key role in adipose tissue metabolism, the regulatory function of TM4SF5 in adipocytes remains unclear. In this study we aimed to establish a TM4SF5 knockout (KO) mouse model and investigated the effects of TM4SF5 KO on mTORC1 signaling–mediated autophagy and mitochondrial metabolism in adipose tissue. TM4SF5 expression was higher in inguinal white adipose tissue (iWAT) than in brown adipose tissue and significantly upregulated by a high-fat diet (HFD). TM4SF5 KO reduced mTORC1 activation and enhanced autophagy and lipolysis in adipocytes. RNA sequencing analysis of TM4SF5 KO mouse iWAT showed that the expression of genes involved in peroxisome proliferator–activated receptor α signaling pathways and mitochondrial oxidative metabolism was upregulated. Consequently, TM4SF5 KO reduced adiposity and increased energy expenditure and mitochondrial oxidative metabolism. TM4SF5 KO prevented HFD-induced glucose intolerance and inflammation in adipose tissue. Collectively, the results of our study demonstrate that TM4SF5 regulates autophagy and lipid catabolism in adipose tissue and suggest that TM4SF5 could be therapeutically targeted for the treatment of obesity-related metabolic diseases.

Adipose tissue is a multiplex connective tissue and a major metabolic site, specialized to store and mobilize lipids (1). It is classified into two main categories: brown adipose tissue (BAT) and white adipose tissue (WAT) (2). BAT contains numerous mitochondria and expresses uncoupling protein 1 (UCP1), which is responsible for the regulation of nonshivering thermogenesis. The catabolism of BAT can be induced in WAT by thermogenic stimulation, such as cold exposure and β3-adrenergic stimulation. This phenomenon is referred to as browning or beiging of WAT (3). Activation of BAT thermogenesis and browning/beiging of WAT have often been investigated as a strategy to increase energy expenditure and reduce adiposity to treat obesity-related metabolic diseases (4–8).

Autophagy is defined as a series of processes that eliminates damaged or unwanted intracellular components and organelles within the lysosomes and is a housekeeping program required for recycling the cytosolic materials (9). The main pathways involved in the regulation of autophagy include the mammalian target of rapamycin complex 1 (mTORC1) and the AMPK pathways. For instance, AMPK activates unc-51 like autophagy activating kinase 1 (ULK1) by phosphorylation at Ser555 (10). In contrast, mTORC1 inhibits ULK1-mediated autophagy by phosphorylation of ULK1 at Ser757 (11). Mechanistically, phosphorylation of ULK1 at Ser757 by mTORC1 prevents the association of ULK1 with AMPK, and thus mTORC1 inhibits AMPK-driven ULK1 activation (11,12).

Autophagy is a significant regulatory process of lipid metabolism in hepatocytes and adipocytes (13). In particular, lipid droplet (LD)-selective autophagy, defined as lipophagy, is an essential catabolic mechanism of LD breakdown in adipocytes (14–16). Furthermore, adipose

[1]College of Pharmacy and Research Institute of Pharmaceutical Sciences, Seoul National University, Seoul, Republic of Korea
[2]Laboratory of Developmental Biology and Genomics, BK21 Plus Program for Advanced Veterinary Science, Research Institute for Veterinary Science, College of Veterinary Medicine, and Korea Mouse Phenotyping Center, Seoul National University, Seoul, Republic of Korea

Corresponding authors: Je Kyung Seong, snumouse@snu.ac.kr, and Yun-Hee Lee, yunhee.lee@snu.ac.kr

Received 17 February 2021 and accepted 22 June 2021

This article contains supplementary material online at https://doi.org/10.2337/figshare.14831082.

C.C. and Y.S. contributed equally to this work.

triglyceride lipase (ATGL) promotes lipophagy, suggesting that cytosolic lipase–dependent lipolysis and autophagy-mediated LD catabolism exhibit complementarity and cooperativity toward lipolysis in adipose tissue and liver (17,18).

Transmembrane 4 L six family member 5 (TM4SF5) is an N-glycosylated plasma membrane protein with four transmembrane domains and is also found in the lysosomal membrane (19). Its regulatory function in actin reorganization, cell adhesion, cell spread, and migration has been reported in relation to the pathogenesis of hepatic diseases, such as fatty liver (19–21). Importantly, TM4SF5 functions as a lysosomal membrane arginine sensor that promotes mTORC1 activation–mediated cell growth (19). TM4SF5 translocates from plasma membrane to lysosomal membrane under arginine sufficient conditions, where it binds sodium-coupled neutral amino acid transporter 9 (SLC38A9), mTORC1, and arginine, enabling arginine efflux for mTORC1 activation (19). Furthermore, overexpression of TM4SF5 facilitates nonalcoholic fatty liver disease and fat accumulation in in vitro hepatocytes and in vivo animal livers (22). Therefore, it is reasonable to hypothesize that TM4SF5 may hamper lipid metabolism through mTORC1-mediated signaling. However, to date, there has been limited investigation on the regulatory roles of TM4SF5 in adipose tissue.

In this study, we explored the roles of TM4SF5 in adipose tissue using a genetic TM4SF5 knockout (KO) model, both in vivo and in vitro. We found that genetic KO increased autophagy, lipolysis, and mitochondrial oxidative metabolism in adipocytes, consequently preventing diet-induced obesity and metabolic dysfunction.

RESEARCH DESIGN AND METHODS

Animals

All animal protocols were approved by the Institutional Animal Care and Use Committee at Seoul National University (SNU190305-1, SNU210520-2) and conducted in strict compliance with the guidelines for humane care and use of laboratory animals specified by the Ministry of Food and Drug Safety. Mice were housed at 22 ± 1°C and maintained on a 12-h light/12-h dark cycle with free access to food and water. Male mice were used for experiments, except for the analysis of the parametrial adipose tissue of female mice.

C57BL6/NTac-Tm4sf5^{em1Krb}/Krb (TM4SF5 KO) mice were established by the CRISPR/Cas9 system with use of single guide RNA (5′-GCTGAGGTTGCCGTCCGTCC**AGG**-3′). The primers used for genotyping are listed in Supplementary Table 1.

For the diet-induced obesity model, mice at 6 weeks of age were fed with a 60% fat diet (D12492; Research Diets, New Brunswick, NJ) for 8 weeks Energy expenditure and food intake were estimated by indirect calorimetry (PhenoMaster; TSE Systems, Bad Homburg, Germany). Body composition was measured by nuclear magnetic resonance scanning EchoMRI-700 (Echo Medical Systems). For the glucose tolerance test, mice were injected with 200 mg/mL D-glucose (2 g/kg body wt i.p.) (G7021; Sigma-Aldrich, St. Louis, MO) (23). For the insulin tolerance test, mice were treated with insulin by injection (0.75 units/kg i.p.) (91077C; Sigma-Aldrich) (23). A glucose meter (Accu-Check Performa, Roche, Basel, Switzerland) was used to measure glucose concentration. For testing of insulin signaling, insulin (0.75 units/kg) was injected into the inferior vena cava and adipose tissues were harvested 10 min later (24). Ex vivo electron transport activity related to mitochondrial oxidative phosphorylation was evaluated by monitoring of the reduction of 0.1% triphenyltetrazolium chloride (TTC) (T8877; Sigma-Aldrich) as described previously (25).

The modified Folch extraction method was used for fecal lipid extraction as previously described (26). Briefly, lipids from feces (1 g per each mouse, collected for 3 days) were extracted with chloroform:methanol solution (2:1) and air-dried for 3 days. For cold tolerance tests, mice were placed in a 4°C cold room and body temperature was measured by rectal thermometry (testo 925; Testo, Lenzkirch, Germany) and infrared camera (FLIR E5 Ex-Series; Teledyne FLIR, Wilsonville, OR) as previously described (23).

Histology

Hematoxylin-eosin (H-E) or immunofluorescence staining was performed with paraffin sections as previously described (27). Adipocyte diameters were determined from the H-E–stained paraffin sections.

Transmission Electron Microscopy

Transmission electron microscopy was performed as previously described (27). Mitochondrial content was analyzed by counting of the numbers of mitochondria per nucleus in ×2,000 magnification images.

Western Blot and Quantitative PCR

Western blot and quantitative PCR (qPCR) were performed as previously described (27). The antibodies used for Western blot are listed in Supplementary Table 2, and primers used for qPCR are listed in Supplementary Table 3.

RNA Sequencing Analysis

cDNA libraries were constructed with the TruSeq Stranded mRNA LT Sample Prep Kit (Illumina, San Diego, USA). The total RNA was sequenced with the NovaSeq 6000 System (Macrogen, Seoul, Republic of Korea). Transcription factors were predicted with use of the Cytoscape plugin iRegulon (version 1.3) as previously described (24). A heat map was generated with the Morpheus program.

Cell Culture

For induction of adipogenic lineage commitment, C3H1 0T1/2 cells (ATCC, Manassas, VA) were exposed to 20∓mg/mL BMP4 (314-BP; R&D systems, Minneapolis, MN) in growth media (DMEM supplemented with 10% FBS) for 3 days. Next, cells were cultured in adipogenic differentiation media (growth media containing 0.125 mmol/L indomethacin [70270; Cayman Chemical, Ann Arbor, MI], 2.5 mmol/L isobutyl methylxanthine [I5879; Cayman Chemical], 1 μmol/L dexamethasone [D4902; Cayman Chemical], 10 μg/mL insulin [I9278; Sigma-Aldrich], and 1 nmol/L triiodothyronine [16028; Cayman]) for 3 days. Then the cells were maintained in growth media containing 10 μg/mL insulin and 1 nmol/L triiodothyronine for 3 days (28). For the chemical inhibition of TM4SF5, 5 μmol/L of 4′-(p-toluenesulfonylamido)-4-hydroxychalcone (TSAHC) (19) was treated for 24 h.

To examine in vitro effects of TM4SF5 KO in adipocytes, we analyzed primary cultures of adipocytes that were differentiated from stromovascular cells obtained from BAT and inguinal WAT (iWAT) of TM4SF5 KO mice as previously described (27). To overexpress GFP- or Myc-fused TM4SF5 in C3H10T1/2 cells, we cloned Tm4sf5 (NM_029360) Mouse ORF Clone (MR201934; OriGene Technologies, Rockville, MD) into pLenti-EF1a-C-mGFP-P2A-Puro Lentiviral Vector (PS100121; OriGene Technologies) or pLenti-EF1a-C-Myc-DDK-P2A-Puro Lentiviral Vector (PS100120; OriGene Technologies) using AsiSI and MluI. Lentiviral particle production and transduction of C3H10T1/2 cells were performed as previously described (29).

Oxygen consumption rate (OCR) was measured with Seahorse XF Analyzers as previously described (28). The coupling efficiency was determined with the following equation: 1 − uncoupled respiration/basal OCR (30,31). Chloroquine (50 μmol/L) (C6628; Sigma-Aldrich) was used as an autophagy inhibitor. We measured glycerol and free fatty acid (FFA) levels in media using glycerol reagent (F6428; Sigma-Aldrich) and HR Series NEFA-HR (2) (Color Reagent A (999-34691); Solvent A (995-34791); Color Reagent B (991-34891); Solvent B (993-35191); NEFA Standard Solution (276-76491) (FUJIFILM Wako Pure Chemicals, Osaka, Japan) according to the manufacturer's instructions.

Immunocytochemistry

Immunocytochemistry was performed as described previously (26). The antibodies for immunocytochemical detection were listed in Supplementary Table 1. DAPI (0.2 μg/mL) (D9542; Sigma-Aldrich), LipidTOX (1:300) (H34477; Invitrogen, Carlsbad, CA), and LysoTracker (1:5,000) (L7525; Invitrogen) were used for nuclei, lipid, and lysosome staining, respectively.

For colocalization analysis, JACoP plugin (ImageJ; National Institutes of Health Bethesda, MD) was used for calculation of the Pearson correlation coefficient (PC). The PC value can range from 1 to −1, with 1 indicating complete colocalization and −1 indicating exclusive staining (32).

Relative mtDNA analysis

Relative mitochondrial DNA (mtDNA) copy number was analyzed as previously described (27). The mtDNA copy number was normalized to nuclear 18S DNA.

Statistical Analysis

Statistical analyses were performed with GraphPad Prism 7 software (GraphPad Software, La Jolla, CA). Data are presented as mean ± SEM. Statistical significance was determined with the unpaired *t* test.

Data and Resource Availability

All data generated or analyzed during this study are included in this article or are available from the corresponding authors on request. The raw RNA-sequencing (RNA-seq) data have been deposited in Gene Expression Omnibus (GEO) (GSE 166303).

RESULTS

Expression of TM4SF5 Was More Abundant in WAT Compared With BAT

We first examined the expression of *Tm4sf5* in adipose tissues from various anatomical locations of mice. In general, *Tm4sf5* transcript levels were higher in WAT compared with BAT and were most abundant in subcutaneous iWAT, among the adipose tissues examined (Fig. 1*A*). Immunoblot analysis confirmed that protein levels of TM4SF5 were higher in iWAT than in BAT (Fig. 1*B*). The publicly available transcriptomics data of mouse adipose tissue consistently showed that *Tm4sf5* expression is higher in iWAT than in BAT (Supplementary Fig. 1*A*: GSE127251). This differential expression of TM4SF5 between BAT and WAT suggests an inverse relationship between TM4SF5 expression and mitochondrial oxidative metabolism in adipose tissue.

Deletion of TM4SF5 Gene Inhibited the mTORC1 Signaling Pathway and Increased Autophagy in Adipose Tissue

To investigate the roles of TM4SF5 in adipose tissue, we established TM4SF5 KO mice using the CRISPR/Cas9 system. TM4SF5 KO was confirmed by immunoblot analysis (Supplementary Fig. 2). Previous studies have reported that TM4SF5 functions as a sensor for lysosomal arginine levels and promotes mTORC1-mediated growth signaling (19). Since mTORC1 activation inhibits macroautophagy, we examined the expression levels of proteins involved in autophagy regulation in the adipose tissue of TM4SF5 KO mice. Immunoblot analysis indicated that the phosphorylation levels of mTOR at Ser2481 and ULK1 at Ser757, which is a downstream target of mTORC1, were reduced in BAT and iWAT of TM4SF5 KO mice (Fig. 2*A* and *B*). However, TM4SF5 KO increased the phosphorylation of ULK1 at Ser555, indicating the activation of autophagy (Fig. 2*B*). Since AMPK phosphorylates ULK1 at Ser555, we examined AMPK activation and found that phosphorylation

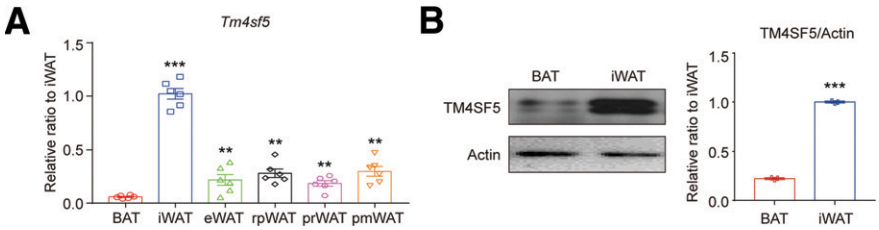

Figure 1—TM4SF5 expression is abundant in subcutaneous WAT compared with BAT. *A*: qPCR analysis of *Tm4sf5* gene expression in BAT, iWAT, epididymal WAT (eWAT), retroperitoneal WAT (rpWAT), perirenal WAT (prWAT), and perimetrial WAT (pmWAT) of mice. Data represent the mean ± SEM of six mice per group (unpaired, two-tailed *t* test, $^{**}P < 0.01$, $^{***}P < 0.001$ vs. BAT). *B*: Immunoblot analysis of TM4SF5 protein in BAT and iWAT of mice. Data represent the mean ± SEM of six mice per group (unpaired, two-tailed *t* test, $^{***}P < 0.001$).

of AMPK at Thr172 was increased by TM4SF5 KO (Fig. 2*A*). This result suggests that TM4SF5 might directly inhibit AMPK activity. Autophagic flux was determined by the ratio of lipidated autophagosome-recruited LC3 (LC3II) to cytosolic LC3 (LC3I) (33), and protein levels of sequestosome-1 (SQSTM1/p62), an autophagy substrate (34). The data indicated that TM4SF5 KO increased the ratio of LC3II to LC3I, and decreased p62 levels in BAT and iWAT, suggesting increased autophagic flux in the adipose tissue of TM4SF5 KO mice (Fig. 2*B*). Since autophagy and lipolysis mechanistically cooperated in adipocytes (35), we examined the protein levels of major lipases in adipose tissue and found the expression of ATGL and phosphorylation of hormone-sensitive lipase (p-HSL) to significantly increase in iWAT and BAT due to TM4SF5 KO (Fig. 2*B*).

To determine the adipocyte-specific roles of TM4SF5 in vitro, we examined autophagic flux in primary adipocytes differentiated from precursor cells isolated from iWAT of TM4SF5 KO mice and wild-type (WT) controls. TM4SF5 KO adipocytes showed upregulated levels of LC3 puncta, indicating increased levels of autophagic flux in TM4SF5 KO mice (Fig. 3*A*). Interestingly, LC3 puncta were closely associated with LD labeled by neutral lipid staining or LD protein perilipin-1 (PLIN1) expression,

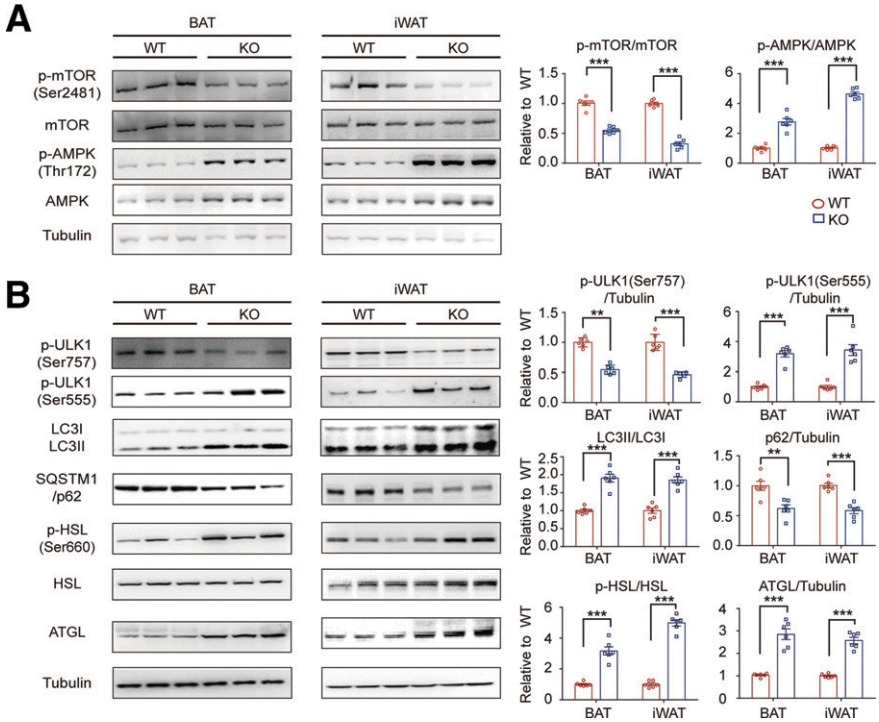

Figure 2—TM4SF5 KO induces autophagy by inhibition of mTOR signaling. *A* and *B*: Immunoblot analysis of p-mTOR (Ser2481), mTOR, p-AMPK (Thr172), AMPK, p-ULK1 (Ser555, Ser757), LC3, SQSTM1/p62, p-HSL (Ser660), HSL, and ATGL proteins in BAT and iWAT of WT and TM4SF5 KO mice. Data represent the mean ± SEM of six mice per group (unpaired, two-tailed *t* test, $^{**}P < 0.01$, $^{***}P < 0.001$).

implying the activation of lipophagy in TM4SF5 KO adipocytes (Fig. 3*A* and *B*). Consistent with the in vivo KO mouse data, p-mTOR (Ser2481) and p-ULK1 (Ser757) levels were reduced by TM4SF5 KO in adipocytes (Fig. 3*C*). An increase in autophagic flux (i.e., reduction in p62 levels) and p-HSL and ATGL levels was observed in TM4SF5 KO adipocytes (Fig. 3*C*).

To capture the dynamic process of autophagy, we introduced chloroquine, an autophagy inhibitor that prevents lysosomal acidification and restrains lysosomal degradation of the autophagosome (33). Consistent with the in vivo data (Fig. 2), immunoblot analysis indicated the levels of LC3II relative to LC3I to be higher in TM4SF5 KO adipocytes than in WT adipocytes under basal conditions (0 h) (Fig. 3*D*). Accumulation of LC3II (increase in LC3II-to-LC3I ratio) with chloroquine treatment was significantly higher in TM4SF5 KO adipocytes than in WT controls (Fig. 3*D*). These data demonstrated that TM4SF5 KO increased autophagy in adipocytes.

To further investigate the roles of TM4SF5 in adipocytes, we established C3H10T1/2 cells overexpressing TM4SF5. TM4SF5 overexpression was confirmed by immunoblot analysis (Supplementary Fig. 3). Staining of lysosomes with LysoTracker indicated that TM4SF5 was

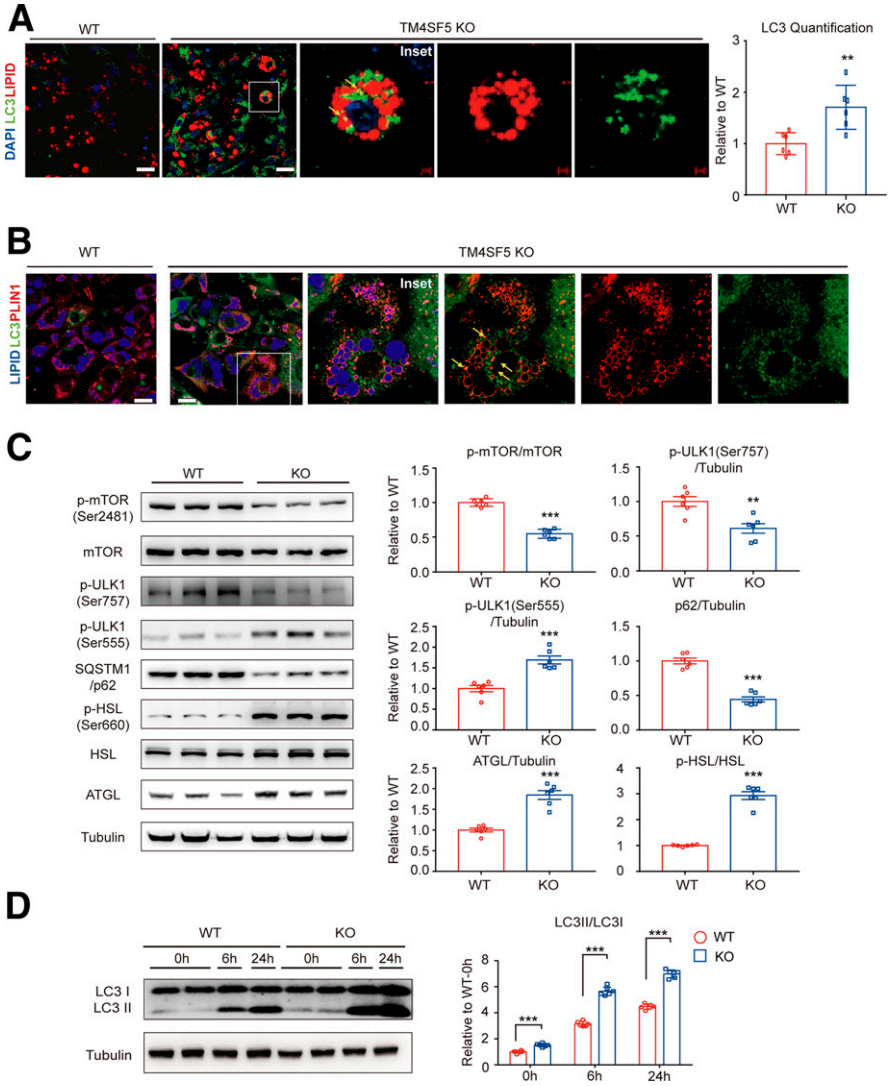

Figure 3—TM4SF5 regulates autophagy activation in adipocytes in vitro. Adipocytes were differentiated from preadipocytes obtained from iWAT of WT and TM4SF5 KO mice. *A*: Representative images of WT and TM4SF5 KO adipocytes immunostained with LC3 along with quantification and higher-magnification view of the boxed region. Neutral lipid and nuclei were counterstained with LipidTOX and DAPI. Size bar = 20 μm. *B*: Representative images of WT and TM4SF5 KO adipocytes immunostained with LC3 and PLIN1. Higher-magnification view of the boxed region is shown. Neutral lipid was counterstained with LipidTOX. Arrows indicate LC3-PLIN1 colocalized locations. Size bar = 20 μm. *C*: Immunoblot analysis of p-mTOR (Ser2481), mTOR, p-ULK1 (Ser555, Ser757), SQSTM1/p62, p-HSL (Ser660), HSL, and ATGL proteins in WT and TM4SF5 KO adipocytes. *D*: Immunoblot analysis of LC3 in WT and TM4SF5 KO adipocytes after 6 and 24 h of chloroquine treatments (50 μmol/L). Data represent the mean ± SEM of six samples per group (unpaired, two-tailed *t* test, $^{**}P < 0.01$, $^{***}P < 0.001$).

located in the lysosomal membrane as well as in the plasma membrane of adipocytes (Fig. 4*A*), which is consistent with previous observations (19). TM4SF5 overexpression reduced the levels of LC3 puncta and the association of LC3 with PLIN1$^+$ LDs (Fig. 4*B*). TM4SF5 overexpression activated the mTORC1 signaling pathway and reduced p-HSL and ATGL levels as well as autophagic flux (Fig. 4*C*). Moreover, TM4SF5 overexpression–mediated activation of the mTORC1 pathway was blocked by treatment with a TM4SF5 inhibitor, TSAHC (19) (Fig. 4*C*).

TM4SF5 KO Upregulated Mitochondrial Content and Activity in Adipose Tissue

Previous studies suggested that autophagy/lipophagy-mediated LD degradation is required for the supply of FFAs to mitochondria (36). Thus, we examined the effects of TM4SF5 KO on mitochondrial protein levels by immunoblot analysis. The results indicated that TM4SF5 KO increased UCP1 in BAT and mitochondrial proteins involved in mitochondrial oxidative phosphorylation (cytochrome c oxidase subunit 4 [COXIV], ubiquinol–cytochrome-c reductase complex core protein 2 [UQCRC2], NADH dehydrogenase ubiquinone 1β subcomplex subunit 8 [NDUFB8], ATP synthase complex 5 [ATP5A], and mitochondrially encoded cytochrome c oxidase I [MTCO1]) in both BAT and iWAT (Fig. 5*A*). The marked increase in mitochondrial mass in BAT and iWAT of TM4SF5 KO mice was validated with electron microscopic analysis (Fig. 5*B*). Moreover, TM4SF5 KO increased the mitochondrial DNA contents of BAT and iWAT (Fig. 5*C*). Next, we measured the electron transport activity related to mitochondrial oxidative phosphorylation in adipose tissues obtained from WT and TM4SF5 KO mice by TTC, a redox indicator stain (37), and found that TM4SF5 KO significantly increased TTC staining in both BAT and iWAT (Fig. 5*D*). In addition, TM4SF5 KO increased association between LC3 and a mitochondrial marker (medium-chain specific acyl-CoA dehydrogenase, mitochondrial [MCAD]), indicating elevated levels of mitophagy (Fig. 5*E*). This observation is consistent with the previous reports demonstrating that phosphorylation of ULK1 at Ser555 by AMPK is required for the induction of mitophagy (10,38).

Since mitochondrial activity in BAT is critical for nonshivering thermogenesis, we examined cold-induced changes in *Tm4sf5* expression in BAT and WAT. qPCR analysis indicated that *Tm4sf5* expression was reduced in iWAT after 3 days of cold exposure (Fig. 5*F*). Next, we sought to determine the effect of TM4SF5 KO on the body temperature and cold sensitivity of the mice. TM4SF5 KO mice maintained higher body temperatures and were more tolerant to cold environments than WT mice (Fig. 5*G* and *H*). Indirect calorimetric analysis indicated the energy expenditure at the basal condition to be higher in TM4SF5 KO mice than WT mice (Fig. 5*I*).

We further analyzed the effects of TM4SF5 KO on mitochondrial contents and oxidative metabolism in primary adipocytes differentiated from preadipocytes isolated from BAT of TM4SF5 KO mice. Consistent with the in vivo data, TM4SF5 KO increased UCP1 and proteins involved in mitochondrial oxidative phosphorylation (Fig. 6*A*). In addition, TM4SF5 KO increased the basal, maximal, and ATP production–linked OCRs (Fig. 6*B*). The coupling efficiency of mitochondrial respiration was not affected by TM4SF5 KO (Fig. 6*B*). We found that the amounts of glycerol and FFA increased in conditioned media from TM4SF5 KO adipocytes (Fig. 6*C* and *D*). Additionally, TM4SF5 overexpression decreased mitochondrial protein levels (i.e., COXIV, ATP5A, and MTCO1) (Fig. 6*E*), which was recovered by the inhibitor TSAHC treatment. TM4SF5 overexpression reduced the release of glycerol and FFA (Fig. 6*F* and *G*). Collectively, in vivo and in vitro data indicated that the genetic deletion of TM4SF5 increased mitochondrial content and mitochondrial oxidative metabolism in adipocytes.

Transcriptomic Characterization of iWAT in TM4SF5 KO Mice

We performed RNA-seq profiling of iWAT from WT and TM4SF5 KO mice. A total of 2,098 genes were found to be differentially regulated in iWAT of TM4SF5 KO mice (Supplementary Fig. 4*A*). One of the brown adipocyte markers, elongation of very-long-chain fatty acid gene 3 [Elovl3]), was upregulated fivefold in iWAT of TM4SF5 KO mice (Supplementary Fig. 4*B*). The top five genes with the highest fold changes included mitochondrial enzymes cytochrome c oxidase subunit 1 (COX1) and cytochrome b (CYTB) (Supplementary Fig. 4*C*). Gene ontology (GO) analysis indicated that the genes involved in mitochondrial fatty acid β-oxidation and electron transport were significantly upregulated in iWAT of KO mice (Supplementary Fig. 4*D*). Downregulated genes in iWAT of TM4SF5 KO mice included mannose receptor C-type 1 (Mrc1), folate receptor 2 (Folr2), and Cd163, which are mainly involved in immune responses (Supplementary Fig. 4*B*). Moreover, GO enrichment analysis identified the peroxisome proliferator–activated receptor (PPAR) signaling pathway to be significantly upregulated by TM4SF5 KO (Supplementary Fig. 4*D*). Transcription factor enrichment analysis by iRegulon also predicted PPARα as the transcriptional factor of 241 upregulated genes (Supplementary Fig. 4*E*). Heat map analysis further illustrated the upregulation of genes involved in PPARα signaling and FFA metabolism in iWAT of TM4SF5 KO mice (Supplementary Fig. 4*F*). Upregulation of the genes involved in PPARα signaling was confirmed by qPCR (Supplementary Fig. 4*G*). According to the results of the Kyoto Encyclopedia of Genes and Genomes (KEGG) pathway analysis, most upregulated genes involved in the PPARα signaling pathway improved fatty acid transport and oxidation, and thermogenesis (Supplementary Fig. 4*H*). According to RNA-seq analysis, we concluded that TM4SF5 KO increased catabolic remodeling of adipose

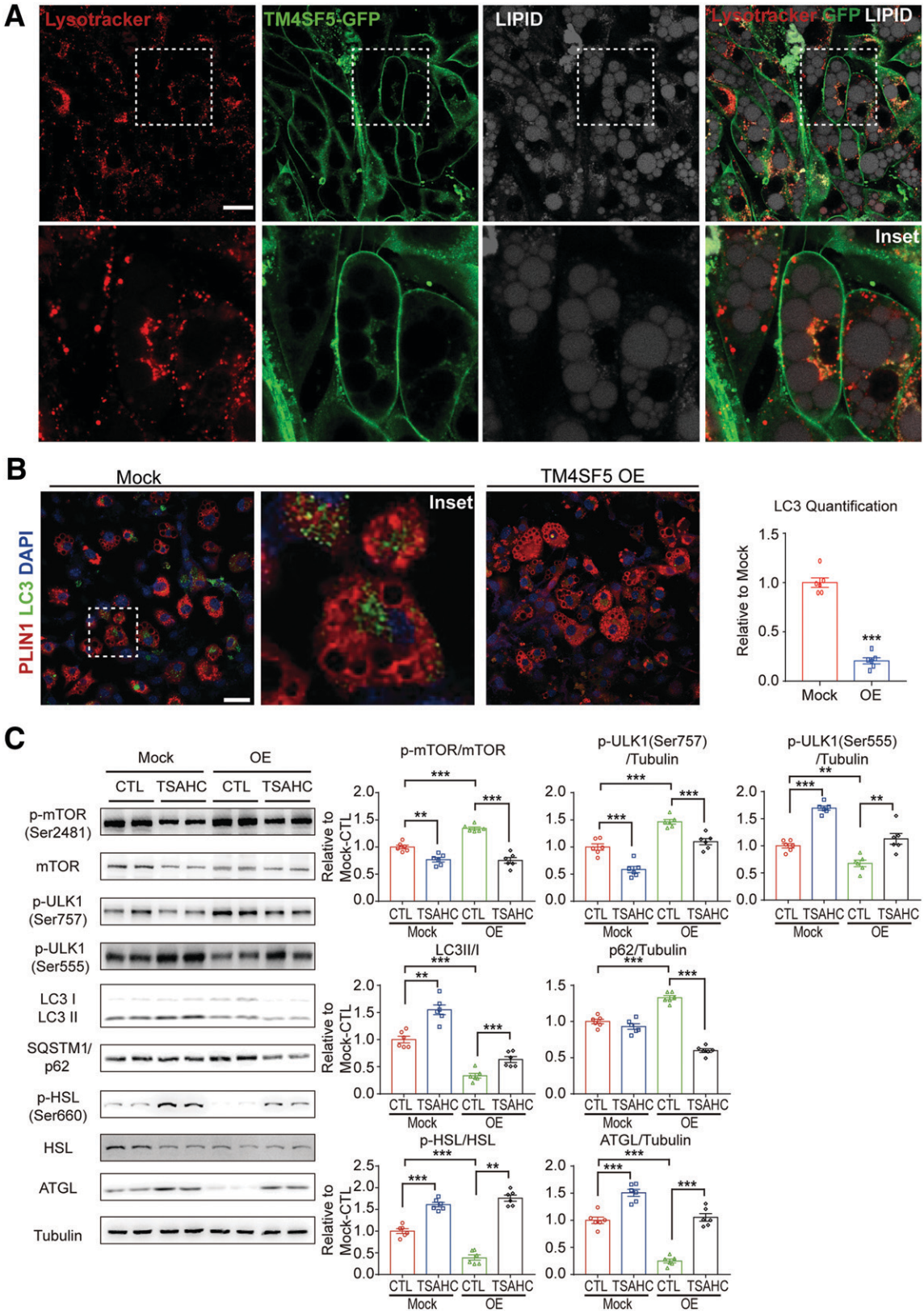

Figure 4—Overexpression of TM4SF5 downregulates autophagy and lipolysis. *A*: Representative image of C3H10T1/2 adipocytes overexpressing GFP-fused TM4SF5. Neutral lipid and lysosome were stained with LipidTOX and LysoTracker. Size bar = 20 μm. *B*: Representative images of C3H10T1/2 adipocytes overexpressing Myc-fused TM4SF5 (OE) and mock control (Mock) stained with LC3 and PLIN1 along with quantification of LC3. Nuclei were counterstained with DAPI. Size bar = 20 μm. C: Immunoblot analysis of p-mTOR (Ser2481), mTOR, p-ULK1 (Ser555, Ser757), SQSTM1/p62, p-HSL (Ser660), HSL, and ATGL proteins in C3H10T1/2 adipocytes overexpressing TM4SF5 and mock controls treated with vehicle (CTL) or 5 μmol/L TSAHC for 24 h. Data represent the mean ± SEM of six samples per group (unpaired, two-tailed *t* test, $^{**}P < 0.01$, $^{***}P < 0.001$).

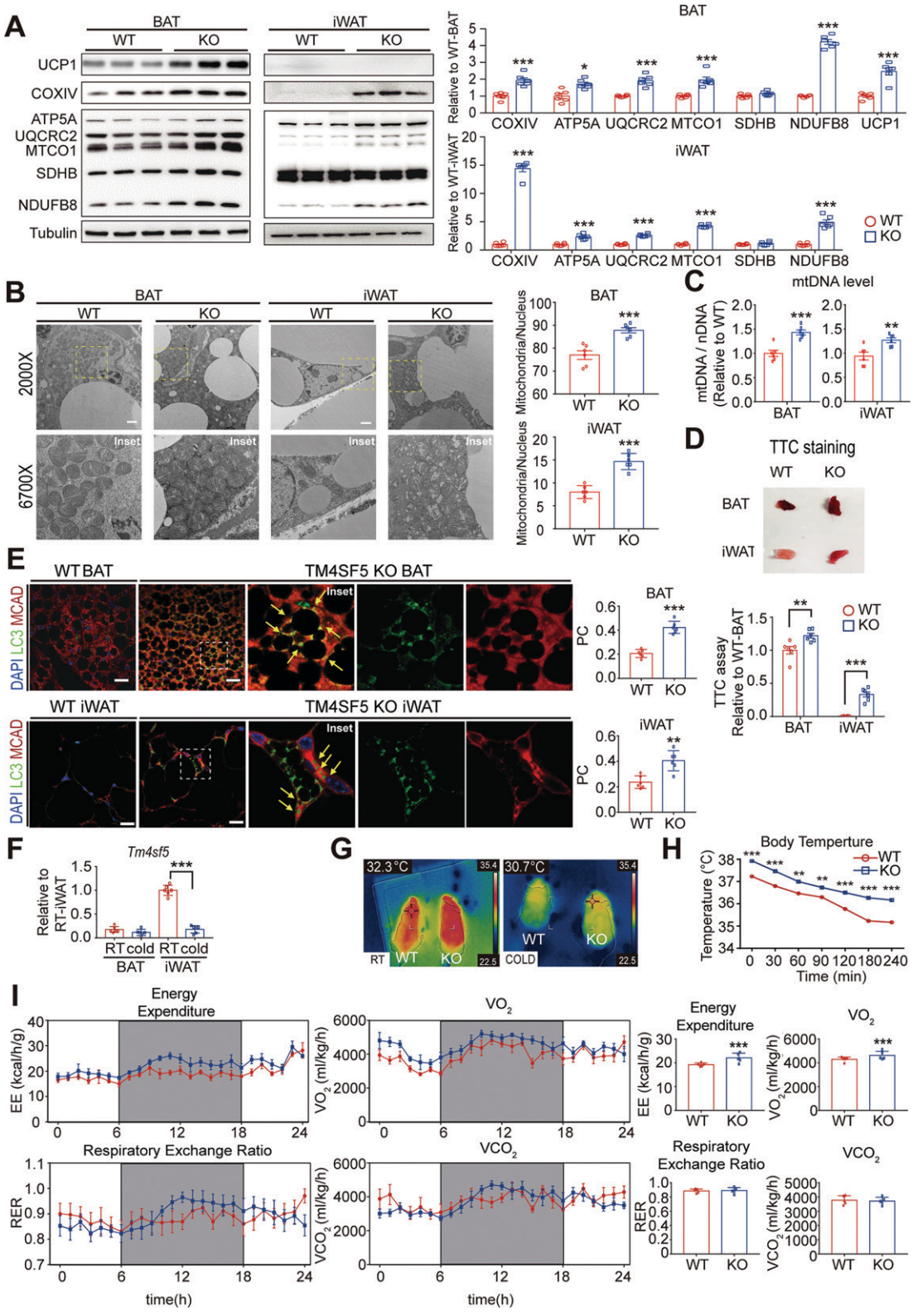

Figure 5—TM4SF5 KO mice manifest catabolic phenotype in adipose tissue. *A*: Immunoblot analysis of UCP1, COXIV, ATP5A, UQCRC2, MTCO1, SDHB, and NDUFB8 proteins in BAT and iWAT of WT and TM4SF5 KO mice. *B*: Representative transmission electron microscopy images from BAT and iWAT of WT and TM4SF5 KO mice along with quantification of mitochondrial content (number of mitochondria per nucleus). Size bar = 2 μm. C: mtDNA content analysis relative to nuclear DNA (nDNA) in BAT and iWAT of WT and TM4SF5 KO mice. *D*: TTC assay in BAT and iWAT of WT and TM4SF5 KO mice. *E*: Representative images of paraffin sections from BAT and iWAT of WT and TM4SF5 KO mice immunostained with MCAD and LC3. Higher-magnification view of boxed region is shown. Colocalization was evaluated with use of ImageJ software via JACoP plugin, and PC values are presented. Size bar = 20 μm. *F*: qPCR analysis of *Tm4sf5*

tissue partly through the upregulation of the PPARα signaling pathway in adipocytes.

TM4SF5 KO Protected Mice From Obesity-Induced Metabolic Dysfunction

To determine the potential involvement of TM4SF5 during overnutrition-induced adipose tissue remodeling, we examined *Tm4sf5* expression in the adipose tissue of mice fed a high-fat diet (HFD) for 8 weeks.

HFD consumption significantly increased *Tm4sf5* gene expression and protein levels in iWAT (Fig. 7*A* and *B*), thus suggesting potential roles of TM4SF5 in the hypertrophic remodeling of adipose tissue. The publicly available transcriptomics data of mouse adipose tissue consistently showed that *Tm4sf5* expression is higher in iWAT of mice fed HFD for 4 weeks (Supplementary Fig. 1*B*: GSE4692). To determine the roles of TM4SF5 in diet-induced obesity, we challenged TM4SF5 KO mice with an HFD and compared their phenotype with WT control mice. Body weights and adiposity (body fat %) of TM4SF5 KO mice were slightly lower than those of WT mice during normal development, when mice were fed a normal chow diet (NCD) (Fig. 7*C* and *D*). HFD-induced increase in body weight and adiposity was lower in TM4SF5 KO mice (Fig. 7*C* and *D*). Consistently, the weight of adipose tissue was lower in TM4SF5 KO mice than in WT controls (Fig. 7*E*). TM4SF5 KO did not affect food consumption or fecal fat content (Supplementary Fig. 6*A* and *B*).

Consistent with previous reports (39), HFD feeding increased the levels of p-mTOR in adipose tissue (Fig. 7*F*). Protein levels of UCP1, COXIV, PPARα, and LC3II/I increased in the BAT and iWAT of HFD-fed TM4SF5 KO mice (Fig. 7*F*). The autophagy substrate, SQSTM1/p62, and the macrophage marker, F4/80, decreased in both BAT and iWAT of HFD-fed TM4SF5 KO mice (Fig. 7*F*). H-E staining indicated the LD size to be smaller in BAT and iWAT of TM4SF5 KO mice (Fig. 7*G*). Consistent with Western blot analysis results, recruitment of $F4/80^+$ macrophages due to HFD reduced in iWAT of TM4SF5 KO mice (Fig. 7*H*).

Moreover, TM4SF5 KO improved glucose tolerance and insulin action in mice fed an HFD, indicated by intraperitoneal glucose and insulin tolerance tests (Fig. 8*A* and *B*). HFD-induced hyperinsulinemia was corrected by TM4SF5 KO (Fig. 8*C*).

TM4SF5 KO mice exhibited decreased levels of serum triglyceride, total cholesterol, and glutamic-pyruvic transaminase (GPT) (Fig. 8*D*). Furthermore, the ability of acute insulin stimulation to increase IRS1/2 and AKT phosphorylation was markedly enhanced in adipose tissue of TM4SF5 KO compared with control WT mice, indicating improved insulin sensitivity (Fig. 8*E*). We confirmed that the suppression of lipolysis by insulin treatment in TM4SF5 KO mice was greater than that in WT mice, as indicated by the reduction in serum FFA and glycerol levels (Fig. 8*F* and *G*). The data collectively demonstrated that TM4SF5 KO protects against diet-induced obesity and metabolic dysfunction.

DISCUSSION

Autophagy involves the regulation of lipid metabolism, and its dysregulation in adipose tissue is associated with the development of metabolic diseases (40). Previous studies have shown that TM4SF5 binds to the arginine transporter, which is required for the activation of the mTORC1 signaling pathway, one of the inhibitory pathways of autophagy (37,41). Therefore, we hypothesized that TM4SF5 could function to regulate adipocyte metabolism by suppressing autophagy through mTORC1 activation in adipocytes. Indeed, the current study demonstrated that TM4SF5 KO increased autophagy activation and mitochondrial lipid metabolism in adipocytes.

The catabolic phenotypes of adipose tissue of TM4SF5 KO mice were beneficial in preventing HFD-induced metabolic dysfunction. For example, TM4SF5 KO mice showed reduced adiposity and improved glucose tolerance and blood lipid profiles. One of the major findings of this study was that TM4SF5 KO increased PPARα signaling, known to stimulate fatty acid oxidation and improve insulin resistance in WAT (42). PPARα signaling is upregulated in iWAT of cold-exposed mice (43). Furthermore, the PPARα agonist WY-14,643 has been shown to be effective in reducing WAT and BAT adiposity and suppressed inflammation in an HFD-induced mouse model (44). Since PPARα was investigated as a target for the activation of lipid catabolism to improve blood lipid profiles, TM4SF5 KO–induced PPARα signaling could be developed into a therapeutic target for clinical application. Although we did not investigate the molecular mechanisms by which TM4SF5 KO affects PPARα signaling, it would be worth further investigation.

TM4SF5 has been studied with a focus on its regulatory roles in the development of liver disease (19) and pulmonary fibrosis (45). Although recent studies have reported that deleting TM4SF5 reduces lipid accumulation in hepatocytes and 3T3-L1 adipocytes (20), studies on the adipocyte-specific roles of TM4SF5 are limited. Based on our findings, further investigations of the regulatory roles of TM4SF5, with a

expression in BAT and iWAT of WT mice after 3 days of cold exposure (4°C, cold). *G* and *H*: Representative image of surface temperature (*G*) and monitoring of rectal temperature (*H*) of WT and TM4SF5 KO mice exposed to cold temperature (4°C) for 4 h with room temperature controls (RT). *I*: Indirect calorimetry analysis of WT and TM4SF5 KO mice. Data represent the mean ± SEM of six mice per group (unpaired, two-tailed *t* test, $*P < 0.05$, $**P < 0.01$, $***P < 0.001$). EE, energy expenditure; RER, respiratory exchange ratio.

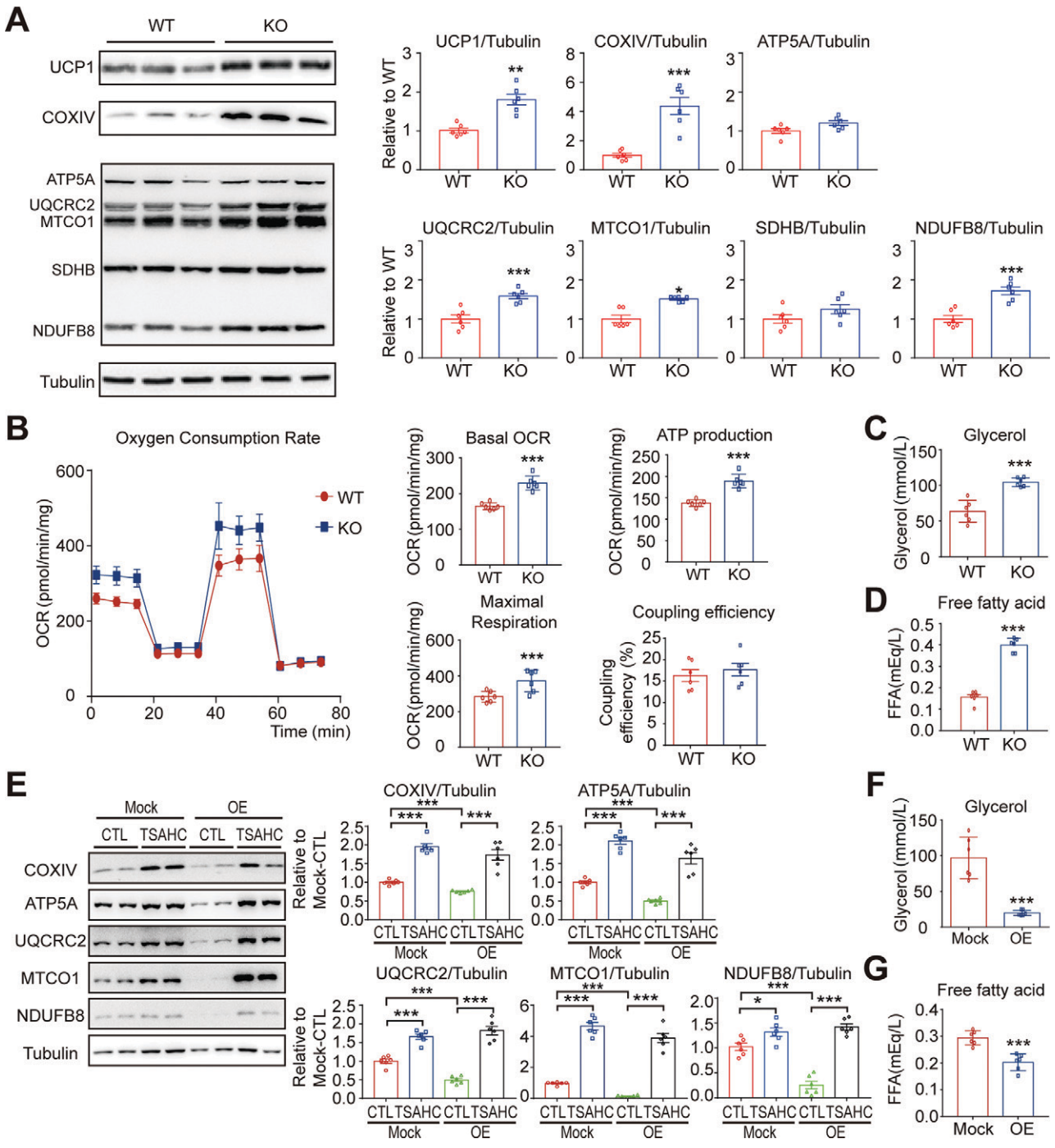

Figure 6—TM4SF5 regulates mitochondrial oxidative metabolism in adipocytes in vitro. *A*: Immunoblot analysis of UCP1, COXIV, ATP5A, UQCRC2, MTCO1, SDHB, and NDUFB8 proteins in WT and TM4SF5 KO adipocytes. Adipocytes were differentiated from preadipocytes obtained from BAT of WT and TM4SF5 KO mice. *B*: OCR analysis of WT and TM4SF5 adipocytes. Adipocytes were differentiated from preadipocytes obtained from iWAT of WT and TM4SF5 KO mice. *C* and *D*: Glycerol (*C*) and FFA (*D*) levels in conditioned media of WT and TM4SF5 KO adipocytes. Adipocytes were differentiated from preadipocytes obtained from iWAT of WT and TM4SF5 KO mice. *E*: Immunoblot analysis of COXIV, ATP5A, UQCRC2, MTCO1, and NDUFB8 proteins in mock controls (Mock) and C3H10T1/2 adipocytes overexpressing TM4SF5 (OE) treated with vehicle control (CTL) or TSAHC (5 μmol/L) for 24 h. *F* and *G*: Glycerol (*F*) and FFA (*G*) levels in conditioned media of mock controls and C3H10T1/2 adipocytes overexpressing TM4SF5. Data represent the mean ± SEM of six samples per group (unpaired, two-tailed *t* test, $*P < 0.05$, $**P < 0.01$, $***P < 0.001$).

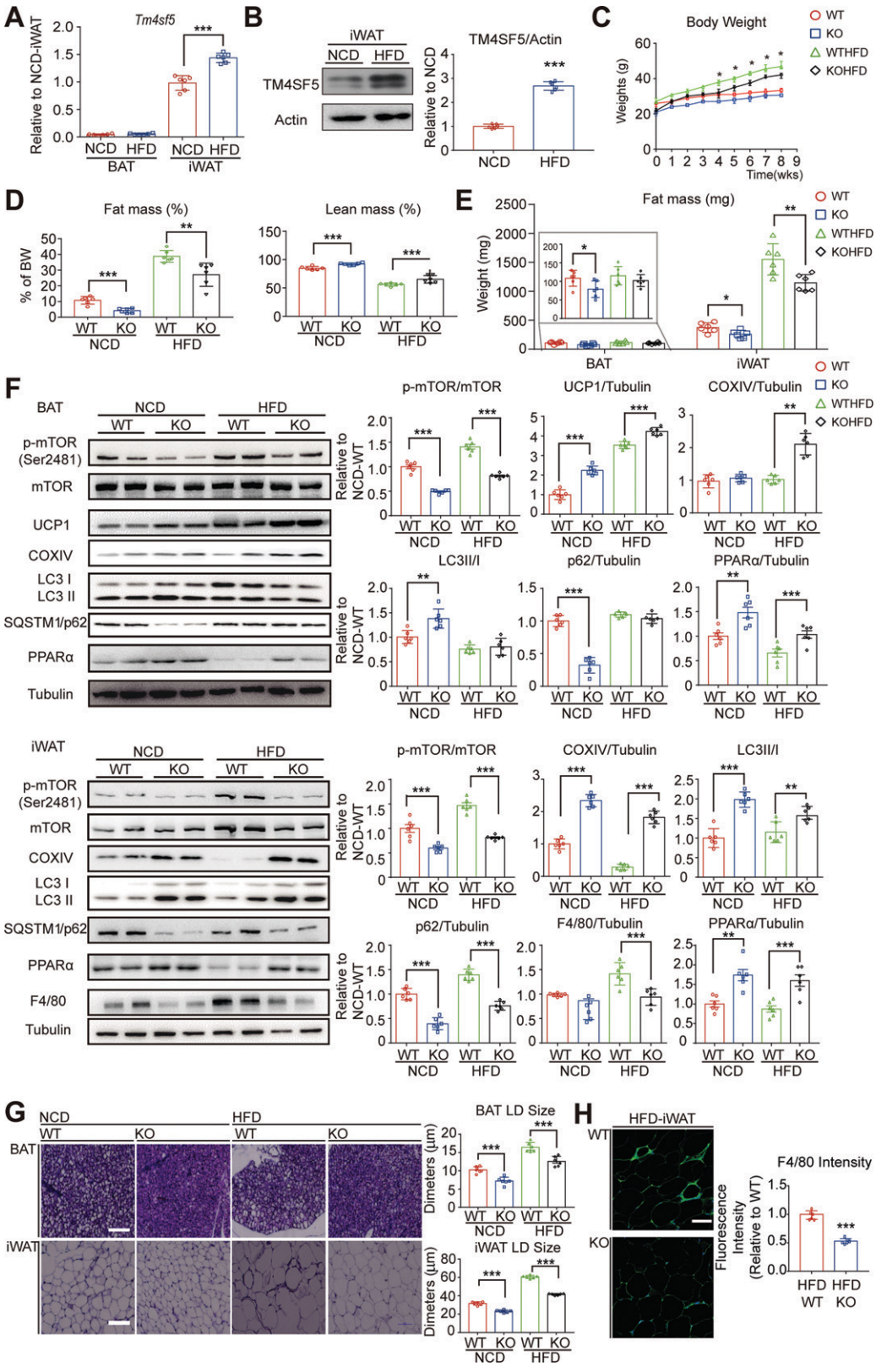

Figure 7—TM4SF5 KO protects mice from obesity-induced metabolic dysfunction. *A*: qPCR analysis of *Tm4sf5* expression in BAT and iWAT of mice after 8 weeks of NCD or HFD feeding. *B*: Immunoblot analysis of TM4SF5 protein in iWAT of mice fed NCD or HFD for 8 weeks. *C–E*: Body weights (*C*), body fat and lean mass (*D*), and adipose tissue weight analysis (*E*) of WT and TM4SF5 KO mice fed with NCD and HFD for 8 weeks. *F*: Immunoblot analysis of p-mTOR (Ser2481), mTOR, UCP1, COXIV, LC3, SQSTM1/p62, PPARα, and F4/80 proteins in BAT and iWAT of WT and TM4SF5 KO mice fed with NCD and HFD for 8 weeks. *G*: Representative images of H-E–stained paraffin sections and LD size quantification from BAT and iWAT of WT and TM4SF5 KO mice fed with NCD or HFD for 8 weeks. Size bar = 100 μm. *H*: Immunofluorescence images of F4/80 in paraffin sections from iWAT of WT and TM4SF5 KO mice fed an HFD for 8 weeks. Size bar = 20 μm. Data represent the mean ± SEM of six mice per group (unpaired, two-tailed *t* test, $*P < 0.05$, $**P < 0.01$, $***P < 0.001$). wks, weeks.

focus on lipid metabolism, are necessary for the therapeutic application of TM4SF5 inhibition in metabolic diseases.

In the current study, we found that TM4SF5 improved obesity-induced inflammation and insulin resistance through the inhibition of the mTORC1 signaling pathway. However, previous studies have demonstrated that mTORC1 inhibition increases ATGL lipolysis and that the adverse effects of uncontrolled activation of lipolysis by mTORC1 KO can lead to insulin resistance and increased plasma TG levels (46–49). These results suggest the possibility that TM4SF5 leads to beneficial metabolic phenotypes through mTORC1-independent pathways, which warrants further investigation.

One limitation of this study was that we investigated the physiological roles of TM4SF5 using a global KO mouse model rather than a tissue-specific KO model. However, the expression of TM4SF5 in WAT was significantly higher than that in other metabolic organs, and the KO did not phenotypically affect other tissues. Due to the high distribution of Tm4sf5 gene expression in the intestine, we

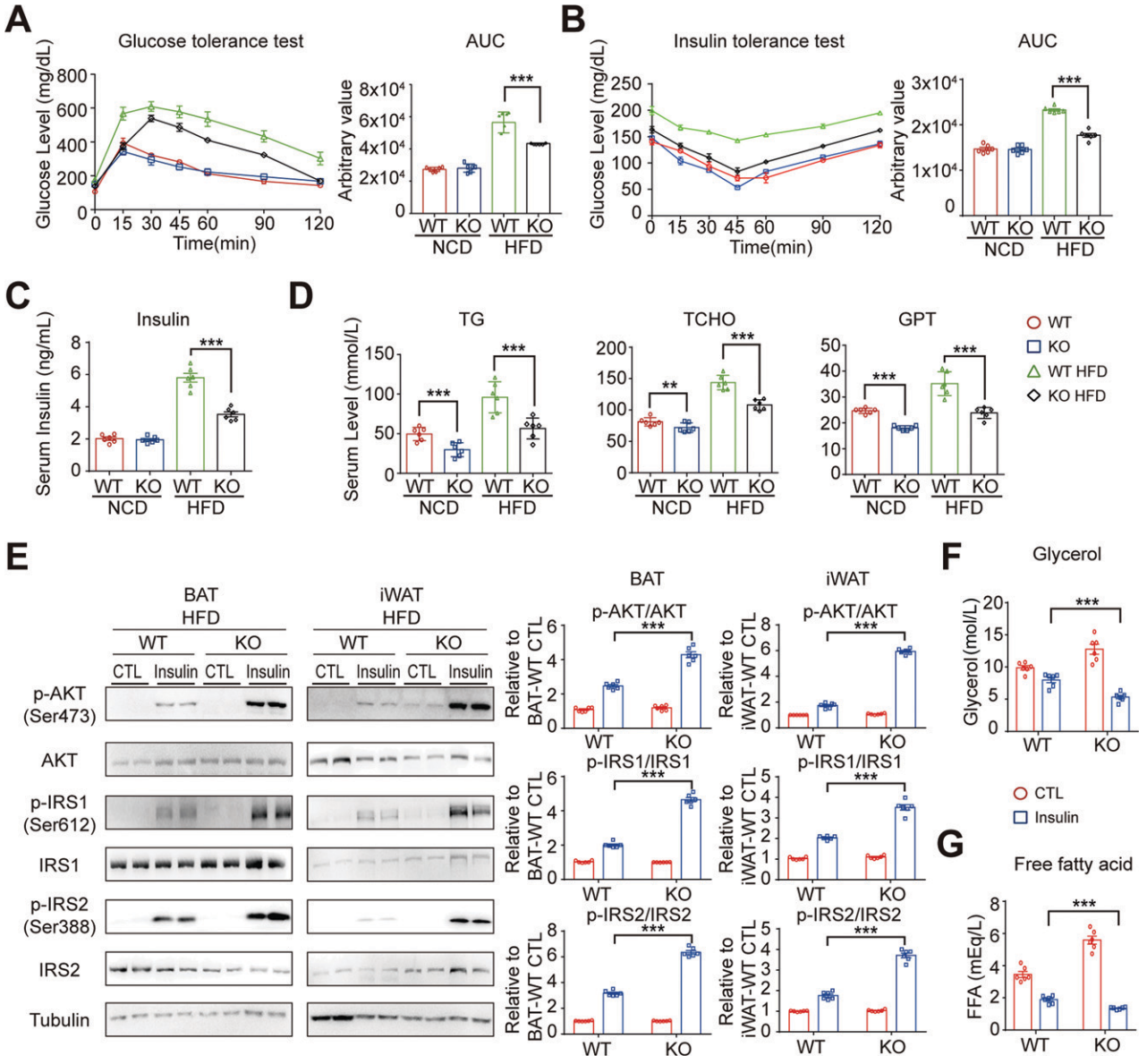

Figure 8—TM4SF5 KO restores insulin sensitivity in mice with HFD-induced obesity. WT and TM4SF5 KO mice were fed the NCD or HFD for 8 weeks. *A* and *B*: Intraperitoneal glucose tolerance test (*A*) and insulin sensitivity test (*B*). AUC, area under the curve. *C* and *D*: insulin (*C*) and triglyceride (TG), total cholesterol (TCHO), and glutamic-pyruvic transaminase (GPT) levels (*D*) in serum. *E*: Immunoblot analysis of p-AKT (Ser473), AKT, p-IRS1 (Ser612), IRS1 and p-IRS2 (Ser388), and IRS2 proteins in BAT and iWAT of WT and TM4SF5 KO mice fed HFD with acute insulin treatment (0.75 units/kg) and controls (CTL) without insulin treatment. *F* and *G*: Glycerol (*F*) and FFA (*G*) levels in serum of WT and TM4SF5 KO mice fed HFD with acute insulin treatment (0.75 units/kg) and controls (CTL) without insulin treatment. Data represent the mean ± SEM of six mice per group (unpaired, two-tailed *t* test, $^{**}P < 0.01$, $^{***}P < 0.001$).

sought to determine the effect of KO on intestinal lipid absorption and found no difference in fecal lipid content between KO and WT mice. Thus, it may be reasonable to conclude that the major effects of TM4SF5 KO manifested in adipose tissue. Although TM4SF5 KO did not affect adipose tissue development or differentiation, TM4SF5 KO mice were more resistant to metabolic challenges, such as overnutrition by HFD feeding, than WT mice. In addition to the in vivo KO mouse study, we established in vitro adipocytes that overexpressed or eliminated TM4SF5 expression and demonstrated the adipocyte-specific effects of TM4SF5 in autophagy and mitochondrial metabolism in adipocytes. Nonetheless, further investigation using adipose tissue–specific conditional KO mice would be required to elucidate the adipose tissue–specific effect of KO.

Collectively, we demonstrated that TM4SF5 KO upregulates autophagy and mitochondrial metabolism in adipose tissue. The beneficial catabolic properties of TM4SF5 KO are associated with PPARα signaling pathways. Therefore, the findings suggest that TM4SF5 could be therapeutically targeted to treat and prevent obesity and obesity-related metabolic diseases.

Funding. This research was supported by National Research Foundation of Korea grants (NRF-2019R1C1C1002014, NRF-2018R1A5A2024425, NRF-2013M3A9D5072550) funded by the Korean government (Ministry of Science and ICT).

Duality of Interest. No potential conflicts of interest relevant to this article were reported.

Author Contributions. Y.-H.L. conceived and designed the study. C.C., Y.S., J.K., Y.K.C., A.S., M.K., H.I., K.K., J.H., J.W.L., and J.K.S. conducted the animal experiments. C.C. and Y.S. performed in vitro experiments. J.W.L. supplied the TSAHC reagent. C.C. and Y.-H.L. wrote the manuscript. All authors reviewed the manuscript. Y.-H.L. is the guarantor of this work and, as such, had full access to all the data in the study and takes responsibility for the integrity of the data and the accuracy of the data analysis.

References

1. Lee YH, Mottillo EP, Granneman JG. Adipose tissue plasticity from WAT to BAT and in between. Biochim Biophys Acta 2014;1842:358–369
2. Saely CH, Geiger K, Drexel H. Brown versus white adipose tissue: a mini-review. Gerontology 2012;58:15–23
3. Ballinger MA, Andrews MT. Nature's fat-burning machine: brown adipose tissue in a hibernating mammal. J Exp Biol 2018;221(Suppl. 1):jeb162586
4. Rui L. Brown and beige adipose tissues in health and disease. Compr Physiol 2017;7:1281–1306
5. Okla M, Kim J, Koehler K, Chung S. Dietary factors promoting brown and beige fat development and thermogenesis. Adv Nutr 2017;8:473–483
6. Hussain MF, Roesler A, Kazak L. Regulation of adipocyte thermogenesis: mechanisms controlling obesity. FEBS J 2020;287:3370–3385
7. Mulya A, Kirwan JP. Brown and beige adipose Tissue: therapy for obesity and its comorbidities? Endocrinol Metab Clin North Am 2016;45:605–621
8. Chouchani ET, Kazak L, Spiegelman BM. New advances in adaptive thermogenesis: UCP1 and beyond. Cell Metab 2019;29:27–37
9. Clemente-Postigo M, Tinahones A, El Bekay R, Malagón MM, Tinahones FJ. The role of autophagy in white adipose tissue function: implications for metabolic health. Metabolites 2020;10:179
10. Egan DF, Shackelford DB, Mihaylova MM, et al. Phosphorylation of ULK1 (hATG1) by AMP-activated protein kinase connects energy sensing to mitophagy. Science 2011;331:456–461
11. Rabanal-Ruiz Y, Otten EG, Korolchuk VI. mTORC1 as the main gateway to autophagy. Essays Biochem 2017;61:565–584
12. Kim J, Kundu M, Viollet B, Guan KL. AMPK and mTOR regulate autophagy through direct phosphorylation of Ulk1. Nat Cell Biol 2011;13:132–141
13. Cairó M, Villarroya J. The role of autophagy in brown and beige adipose tissue plasticity. J Physiol Biochem 2020;76:213–226
14. Dong H, Czaja MJ. Regulation of lipid droplets by autophagy. Trends Endocrinol Metab 2011;22:234–240
15. Liu K, Czaja MJ. Regulation of lipid stores and metabolism by lipophagy. Cell Death Differ 2013;20:3–11
16. Ro SH, Jang Y, Bae J, Kim IM, Schaecher C, Shomo ZD. Autophagy in adipocyte browning: emerging drug target for intervention in obesity. Front Physiol 2019;10:22
17. Martinez-Lopez N, Garcia-Macia M, Sahu S, et al. Autophagy in the CNS and periphery coordinate lipophagy and lipolysis in the brown adipose tissue and liver. Cell Metab 2016;23:113–127
18. Sathyanarayan A, Mashek MT, Mashek DG. ATGL promotes autophagy/lipophagy via SIRT1 to control hepatic lipid droplet catabolism. Cell Rep 2017;19:1–9
19. Jung JW, Macalino SJY, Cui M, et al. Transmembrane 4 L six family member 5 senses arginine for mTORC1 signaling. Cell Metab 2019;29:1306–1319.e7
20. Ryu J, Kim E, Kang M-K, et al. Differential TM4SF5-mediated SIRT1 modulation and metabolic signaling in nonalcoholic steatohepatitis progression. J Pathol 2021;25355–67
21. Ryu J, Lee JW. TM4SF5-mediated roles in the development of fibrotic phenotypes. Mediators Inflamm 2017;2017:5108525
22. Kim SN, Kwon HJ, Im SW, et al. Connexin 43 is required for the maintenance of mitochondrial integrity in brown adipose tissue. Sci Rep 2017;7:7159
23. Ying W, Riopel M, Bandyopadhyay G, et al. Adipose tissue macrophage-derived exosomal miRNAs can modulate in vivo and in vitro insulin sensitivity. Cell 2017;171:372–384.e12
24. Li P, Zhu Z, Lu Y, Granneman JG. Metabolic and cellular plasticity in white adipose tissue II: role of peroxisome proliferator-activated receptor-alpha. Am J Physiol Endocrinol Metab 2005;289:E617–E626
25. Kraus D, Yang Q, Kahn BB. Lipid extraction from mouse feces. Bio Protoc 2015;5:e1375
26. Son Y, Cho YK, Saha A, et al. Adipocyte-specific Beclin1 deletion impairs lipolysis and mitochondrial integrity in adipose tissue. Mol Metab 2020;39:101005
27. Kim S-N, Kwon H-J, Akindehin S, Jeong HW, Lee Y-H. Effects of epigallocatechin-3-gallate on autophagic lipolysis in adipocytes. Nutrients 2017;9:680
28. Cho YK, Son Y, Saha A, et al. STK3/STK4 signalling in adipocytes regulates mitophagy and energy expenditure. Nat Metab 2021;3:428–441
29. Dott W, Mistry P, Wright J, Cain K, Herbert KE. Modulation of mitochondrial bioenergetics in a skeletal muscle cell line model of mitochondrial toxicity. Redox Biol 2014;2:224–233
30. Isono T, Chano T, Yonese J, Yuasa T. Therapeutic inhibition of mitochondrial function induces cell death in starvation-resistant renal cell carcinomas. Sci Rep 2016;6:25669
31. Bolte S, Cordelières FP. A guided tour into subcellular colocalization analysis in light microscopy. J Microsc 2006;224:213–232
32. Mizushima N, Yoshimori T, Levine B. Methods in mammalian autophagy research. Cell 2010;140:313–326
33. Liu WJ, Ye L, Huang WF, et al. p62 links the autophagy pathway and the ubiqutin-proteasome system upon ubiquitinated protein degradation. Cell Mol Biol Lett 2016;21:29

34. Zechner R, Madeo F, Kratky D. Cytosolic lipolysis and lipophagy: two sides of the same coin. Nat Rev Mol Cell Biol 2017;18:671–684
35. Kloska A, Węsierska M, Malinowska M, Gabig-Cimińska M, Jakóbkiewicz-Banecka J. Lipophagy and lipolysis status in lipid storage and lipid metabolism diseases. Int J Mol Sci 2020;21:6113
36. Kwon HJ, Saha A, Ahn SY, et al. Polymethoxyselenoflavones exert anti-obesity effects through activation of lipolysis and brown adipocyte metabolism. Int J Obes 2021;45:122–129
37. Laker RC, Drake JC, Wilson RJ, et al. Ampk phosphorylation of Ulk1 is required for targeting of mitochondria to lysosomes in exercise-induced mitophagy. Nat Commun 2017;8:548
38. Khamzina L, Veilleux A, Bergeron S, Marette A. Increased activation of the mammalian target of rapamycin pathway in liver and skeletal muscle of obese rats: possible involvement in obesity-linked insulin resistance. Endocrinology 2005;146:1473–1481
39. Ferhat M, Funai K, Boudina S. Autophagy in adipose tissue physiology and pathophysiology. Antioxid Redox Signal 2019;31:487–501
40. Rabanal-Ruiz Y, Korolchuk VI. mTORC1 and nutrient homeostasis: the central role of the lysosome. Int J Mol Sci 2018;19:818
41. Goto T, Lee JY, Teraminami A, et al. Activation of peroxisome proliferator-activated receptor-alpha stimulates both differentiation and fatty acid oxidation in adipocytes. J Lipid Res 2011;52:873–884
42. Defour M, Dijk W, Ruppert P, Nascimento EBM, Schrauwen P, Kersten S. The peroxisome proliferator-activated receptor α is dispensable for cold-induced adipose tissue browning in mice. Mol Metab 2018;10:39–54
43. Tsuchida A, Yamauchi T, Takekawa S, et al. Peroxisome proliferator–activated receptor (PPAR)α activation increases adiponectin receptors and reduces obesity-related inflammation in adipose tissue: comparison of activation of PPARα, PPARγ, and their combination. Diabetes 2005;54:3358–3370
44. Kim JE, Kim HJ, Jung JW, et al. TM4SF5-mediated CD44v8-10 splicing variant promotes survival of type II alveolar epithelial cells during idiopathic pulmonary fibrosis. Cell Death Dis 2019;10:645
45. Tory R, Sachs-Barrable K, Hill JS, Wasan KM. Cyclosporine A and rapamycin induce in vitro cholesteryl ester transfer protein activity, and suppress lipoprotein lipase activity in human plasma. Int J Pharm 2008;358:219–223
46. Paolella LM, Mukherjee S, Tran CM, et al. mTORC1 restrains adipocyte lipolysis to prevent systemic hyperlipidemia. Mol Metab 2020;32:136–147
47. Pereira MJ, Palming J, Rizell M, et al. The immunosuppressive agents rapamycin, cyclosporin A and tacrolimus increase lipolysis, inhibit lipid storage and alter expression of genes involved in lipid metabolism in human adipose tissue. Mol Cell Endocrinol 2013;365:260–269
48. Blanchard PG, Festuccia WT, Houde VP, et al. Major involvement of mTOR in the PPARγ-induced stimulation of adipose tissue lipid uptake and fat accretion. J Lipid Res 2012;53:1117–1125